JACS
JOURNAL OF THE AMERICAN CHEMICAL SOCIETY
Article
pubs.acs.org/JACS

Boosting Hot-Electron Generation: Exciton Dissociation at the Order–Disorder Interfaces in Polymeric Photocatalysts

Hui Wang,[†] Xianshun Sun,[†] Dandan Li,[‡] Xiaodong Zhang,*[,†] Shichuan Chen,[†] Wei Shao,[†] Yupeng Tian,[‡] and Yi Xie*[,†]

[†]Hefei National Laboratory for Physical Science at the Microscale, Collaborative Innovation Center of Chemistry for Energy Materials, University of Science and Technology of China, Hefei, Anhui 230026, People's Republic of China

[‡]Department of Chemistry, Anhui University, Hefei, Anhui 230039, People's Republic of China

Supporting Information

ABSTRACT: Excitonic effects, arising from the Coulomb interactions between photogenerated electrons and holes, dominate the optical excitation properties of semiconductors, whereas their influences on photocatalytic processes have seldom been discussed. In view of the competitive generation of excitons and hot carriers, exciton dissociation is proposed as an alternative strategy for hot-carrier harvesting in photocatalysts. Herein, by taking heptazine-based melon as an example, we verified that enhanced hot-carrier generation could be obtained in semicrystalline polymeric photocatalysts, which is ascribed to the accelerated exciton dissociation at the abundant order–disorder interfaces. Moreover, driven by the accompanying electron injection toward ordered chains and hole blocking in disordered chains, semicrystalline heptazine-based melon showed an ~7-fold promotion in electron concentration with respect to its pristine counterpart. Benefiting from these, the semicrystalline sample exhibited dramatic enhancements in electron-involved photocatalytic processes, such as superoxide radical production and selective alcohol oxidation. This work brightens excitonic aspects for the design of advanced photocatalysts.

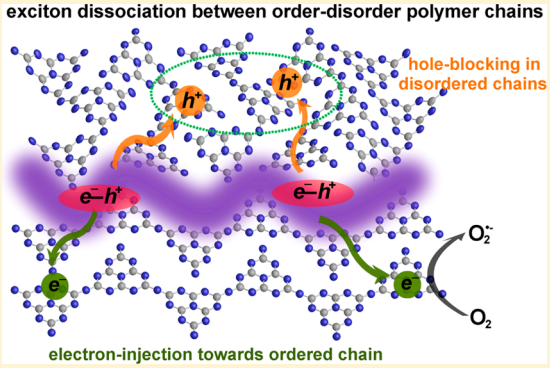

INTRODUCTION

Ever since the concept of the exciton was first proposed in 1931, great efforts have been devoted to excitonic research on semiconductors, establishing intriguing applications in numerous optoelectronic fields such as photovoltaic cells, field-effect transistors, organic light emitting diodes, and so on.[1−5] Since excitons are bound electron–hole pairs formed by attractive Coulomb interactions, excitonic effects should be taken into account for all optical aspects of semiconductors. Unfortunately, extensive excitonic studies of some significant optical excitation processes have long been neglected. Photocatalysis, a typical photoexcitation process that has been widely studied for its potential in solving the energy crisis and environmental pollution, is believed to be closely related to the photogenerated charges (that is, hot electrons and holes),[6−8] whereas the excitonic aspects of photocatalysts have rarely been realized. For instance, optimizations of band structures and charge separations are currently accepted as the most efficient strategies for the regulation of hot-carrier generation in photocatalysts,[7,8] but these are not comprehensive once the competitive exciton generation (with respect to hot-carrier generation) is taken into account. Besides, the strong interactions among excitons, such as exciton–exciton annihilation, also serve as shackles for hot-carrier generation.[9,10] In this regard, gaining a deeper understanding of the excitonic aspects of photocatalytic processes is urgently required for the design of advanced photocatalysts. On the basis of the component of the bound electron and hole, we deduce that the dissociation of an exciton into a hot electron and hole would be an alternative strategy for hot-carrier harvesting in photocatalysts. To this end, we focus on a booming kind of photocatalysts, polymeric semiconductors, whose generally low dielectric properties imply potentially rich excitons. For instance, the heptazine-based melon (nominally, polymeric carbon nitride), a promising polymeric photocatalyst composed of melon chains, has attracted great interest ever since its discovery.[11−14] Just recently, we have demonstrated the strong exciton effects and robust excitonic interactions in this well-known photocatalyst, enabling us to interrogate the excitonic aspects for photocatalytic processes.[15]

Given that hot excitons tend to dissociate into free charges at the area with a disordered energy landscape,[16,17] we deduce that enhanced charge-carrier generation would be expected in structures with abundant order–disorder interfaces. In addition, density functional theory (DFT) simulations (Figure 1a) demonstrate that the ordered heptazine-based chain possesses slightly reduced highest occupied molecular orbital (HOMO)

Received: December 14, 2016
Published: January 19, 2017

DOI: 10.1021/jacs.6b12878
J. Am. Chem. Soc. 2017, 139, 2468–2473

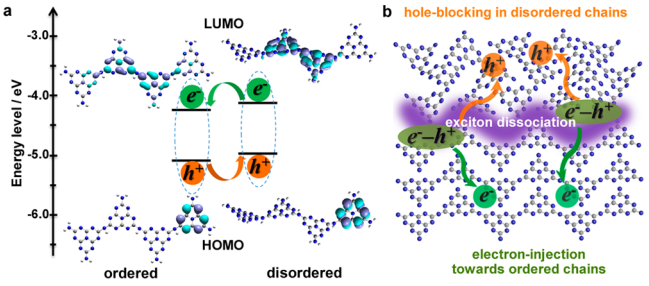

Figure 1. (a) DFT simulations of ordered and disordered heptazine-based chains. Inset: corresponding charge-carrier transfer behaviors (blue balls, nitrogen atoms; gray balls, carbon atoms). (b) Schematic illustration of exciton dissociation and charge transfer in semicrystalline heptazine-based melon.

and lowest unoccupied molecular orbital (LUMO) energy levels (−6.20 and −3.51 eV, respectively) with respect to the disordered chain (−6.12 and −3.34 eV for HOMO and LUMO, respectively). The lower HOMO and LUMO energy levels can facilitate electron injection toward ordered chains and hole blocking in disordered chains,[18] resulting in selective extraction of electrons from the melon matrix. Moreover, the highly conjugated character of the ordered chains would favor electron transport, accelerating electron migration toward the surface for electron-involved photocatalytic processes (as shown schematically in Figure 1b). It should be noted that the intriguing charge flow is quite similar to that in heterostructured carbon nitride,[19−21] where directional migration of hot carriers occurs at the interface between two different semiconductors (or metal−semiconductor) with suitable band structures. Nevertheless, the charge flow regulation at the order−disorder interface in a semicrystalline sample is free of any incorporated heteromaterials, mainly depending on the degree of stretching of the polymer chains, which probably could be denoted as homojunctions.

Here, by taking heptazine-based melon as an example, we propose that semicrystalline polymers that contain abundant order−disorder interfaces possess significantly boosted exciton dissociation (for both spin singlet and triplet). Benefiting from the unique structure, semicrystalline heptazine-based melon (SC-HM) exhibits a 7-fold promotion of the free electron concentration with respect to the pristine counterpart, thereby facilitating electron-involved photocatalytic processes like molecular oxygen activation and selective aerobic oxidation.

EXPERIMENTAL SECTION

Preparation of Pristine Heptazine-Based Melon (pristine-HM). Melamine (10 g) was put into a ceramic crucible (30 mL) with a cover and then heated at 600 °C for 10 h in a muffle furnace with a ramp rate of ∼10 °C/min for both the heating and cooling processes. After they were fully ground and washed, the yellow powder samples were collected and denoted as pristine-HM.

Preparation of Semicrystalline Heptazine-Based Melon. Semicrystalline samples were prepared through a chloride-ion-assisted hydrothermal method. In detail, 200 mg of pristine-HM and 1 g of ammonium chloride were fully ground for 10 min. The mixture was then transferred to a Teflon cup (30 mL) containing 20 mL of distilled water and heated in a sealed autoclave at 180 °C for 24 h. After being cooled down, the product was collected, washed with water several times, and dried under vacuum for further analysis. This material is denoted as SC-HM.

Preparation of Annealed Semicrystalline Heptazine-Based Melon. The annealed SC-HM sample was prepared through a rapid annealing treatment. In detail, 100 mg of SC-HM was pressed into tablets and put into a quartz boat. The boat was then heated at 500 °C under an argon atmosphere for 2 min and then cooled to room temperature. The collected product was ground for further analysis.

Molecular Oxygen Activation Measurements. A 20 μL aliquot of an aqueous suspension of the sample (4 g L^{-1}) and 20 μL of 3,3′,5,5′-tetramethylbenzidine (TMB) (50 mM aqueous solution) were injected into 2 mL of HAc/NaAc buffer solution. A xenon lamp (PLS-SXE300/300UV, Trusttech Co., Ltd., Beijing) without a filter was used as the light source. TMB oxidation was estimated by monitoring the absorbance around 380 nm with a UV−vis spectrophotometer. For scavenger tests, different amounts of scavengers (carotene, 2 mg; mannitol, 50 mM, 100 μL; catalase, 4000 units/mL, 100 μL; SOD, 4000 units/mL, 100 μL) were added to identify the active oxygen species.

Electron Spin Resonance Trapping Measurements. A 50 μL aliquot of an aqueous suspension of the sample (2 g L^{-1}) was mixed with 500 μL of trapping agent solution (50 mM). After being illuminated for 30 s, the mixture was characterized using a Bruker EMX plus model spectrometer operating at the X-band frequency (9.4 GHz) at room temperature.

Characterizations. X-ray diffraction (XRD) characterizations were carried out on a Philips X'Pert Pro Super diffractometer with Cu Kα radiation (λ = 1.54178 Å). X-ray photoelectron spectroscopy (XPS) was performed on an ESCALAB MKII spectrometer with a Mg Kα excitation source (hν = 1253.6 eV). High-resolution transmission electron microscopy (HRTEM) images were recorded on a JEM-2100F field-emission electron microscope at an acceleration voltage of 200 kV. UV−vis spectra were acquired on a PerkinElmer Lambda 950 UV−vis−NIR spectrophotometer. Fourier transform infrared (FT-IR) spectra were obtained on a Magna-IR750 FT-IR spectrometer in a KBr pellet, scanning from 4000 to 400 cm^{-1} at room temperature. Differential scanning calorimetry (DSC) analyses were carried out on a TA Instruments DSC Q2000 device with a heating rate of 5 °C min^{-1} under an atmosphere of N_2. X-ray absorption spectroscopy (XAS) at the carbon K edge was performed on beamline U19 at the National Synchrotron Radiation Laboratory, China. NMR experiments were performed with a 400 MHz Bruker AVANCE AV III NMR spectrometer. The steady-state fluorescence and phosphorescence spectra as well as the time-resolved phosphorescence spectra were acquired on a FLUOROLOG-3-TAU fluorescence spectrometer equipped with an integrating sphere. The nanosecond-domain time-resolved fluorescence spectra were measured on a FLS920 fluorescence spectrometer (Edinburgh Instruments Ltd.). The electrochemical measurements were performed on an electrochemical workstation (CHI760E, Shanghai Chenhua Limited, China).

Calculations. All of the calculations were done with the Gaussian 03 suite of programs. No constraints to bonds/angles/dihedral angles were applied in the calculations, and all of the atoms were free to optimize. The electronic transition energies and corresponding oscillator strengths were calculated with time-dependent density functional theory (TD-DFT) at the B3LYP/6-31G** level.

RESULTS AND DISCUSSION

In this study, semicrystalline heptazine-based melon (SC-HM) was synthesized through a hydrothermal process (see details in the Supporting Information). The XRD pattern of pristine heptazine-based melon (pristine-HM) exhibited two pattern peaks located at 13.1° and 27.6° (Figure 2a), which could be indexed as the (100) interplanar structural packing peak and the (002) interlayer stacking peak, respectively. For SC-HM, the sharpened and reinforced peaks suggest the enhanced crystallinity and periodicity of the sample. The (100) peak shifted to a lower diffraction angle of 10.9°, revealing the extended interplanar packing distance of about 8.2 Å compared with 6.8 Å for pristine-HM. The narrower (002) diffraction peak at 28.0° suggests the compacted packing and planarization of undulated melon chains of SC-HM (as shown schematically in Figure 2b).[22] As displayed in Figure 2c, C 1s XPS spectra

DOI: 10.1021/jacs.6b12878
J. Am. Chem. Soc. 2017, 139, 2468−2473

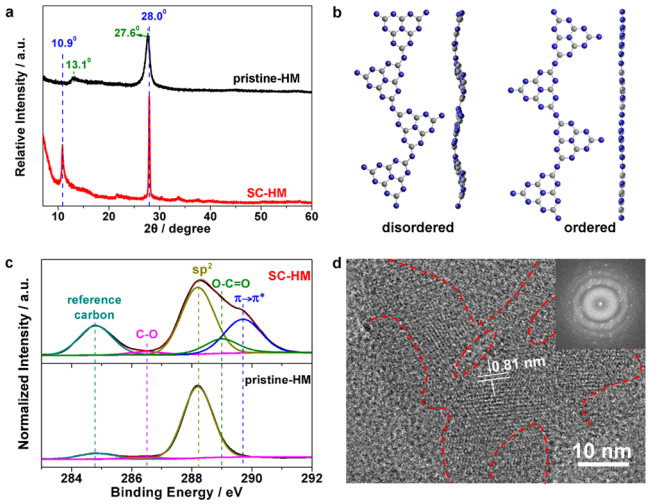

Figure 2. (a) XRD patterns. (b) Structural schematic diagram of disordered and ordered heptazine-based chains (blue balls, nitrogen atoms; gray balls, carbon atoms). (c) C 1s XPS spectra of pristine-HM and SC-HM. (d) HRTEM image of SC-HM (inset: corresponding Fourier transform pattern).

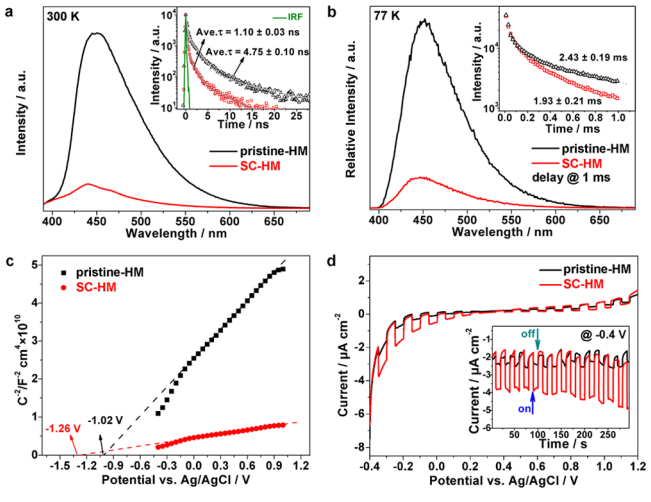

Figure 3. (a) Steady-state fluorescence spectra at 300 K (inset: time-resolved fluorescence kinetics monitoring at the corresponding emission peaks), (b) steady-state delayed fluorescence spectra at 77 K with a 1 ms delay (inset: time-resolved delayed fluorescence kinetics monitoring at the corresponding emission peaks), (c) Mott−Schottky curves, and (d) potential-bias-dependent photocurrent measurements (inset: photocurrent transient response at −0.4 V vs Ag/AgCl, pH 6.6) for pristine-HM (black) and SC-HM (red).

suggest that apart from the divided peaks centered at 284.6, 288.2, and 286.5 eV, assigned to the standard reference carbon, sp^2-bonded carbon, and C−O, respectively, the broadened C 1s spectrum of SC-HM could be attributed to two new energy contributions centered at 289.0 and 289.7 eV. The former peak was assigned to −COOH, while the latter would be indexed to a shakeup satellite due to the carbon $\pi-\pi^*$ transition,[23] which further suggests enhanced conjugation arising from the ordered melon chains. Besides, the purity of the sample was also confirmed by XPS spectra (Figure S1). The FT-IR spectra (Figure S2) indicate that compared with pristine-HM, SC-HM retains the heptazine-based structure, while some novel deformations (strengthened or splitting) of the bands suggest the promoted polymeric orientation and crystallinity. HRTEM offers an intuitive observation of order−disorder interfaces in SC-HM. As shown in Figures 2d and S3, obvious lattice fringes surrounded by amorphous domains were found; the interfaces between ordered and disordered regions are marked with red dashed lines. These features, to some extent, might indicate the homojunction structure of the obtained semicrystalline sample. The corresponding Fourier transform pattern clearly presents the diffraction spots within rings, revealing the coexistence of ordered and disordered chains in SC-HM. As one of the most effective methods for determining the crystallinity of polymers, DSC analyses were carried out, presenting a distinct strong thermal relaxation stage in SC-HM that could be assigned to the "melt" of the crystallites (Figure S5). Moreover, X-ray absorption spectroscopy, an effective method for characterization of local atomic environments, demonstrated the presence of a graphitic interlayer state in SC-HM (Figure S6), giving further evidence for the promoted crystallinity. On the basis of the above results, we conclude that the semicrystalline heptazine-based melon with abundant order−disorder interfaces was successfully prepared.

The unique semicrystalline feature is supposed to greatly impact the optical excitation processes in SC-HM. Photoluminescence measurements were performed to investigate the involved excitonic processes. Figure 3a displays the steady-state prompt fluorescence spectra recorded at 300 K, which show that SC-HM exhibits a slightly blue-shifted but significantly reduced emission (peaked at ∼437 nm) with respect to pristine-HM (peaked at ∼450 nm). As prompt fluorescence arises from radiative decay of singlet excitons in the heptazine-based matrix, the remarkable intensity difference reveals the notably reduced population of singlet excitons. Time-resolved fluorescence spectra monitored at the corresponding steady-state emission peaks yield mean radiative lifetimes of ∼4.75 and ∼1.10 ns for pristine-HM and SC-HM, respectively (the lifetime components are listed in Table S1). The dramatically reduced singlet exciton lifetime clearly suggests enhanced singlet exciton dissociation in the semicrystalline case. Delayed fluorescence measurements were further carried out to interrogate the case of triplet excitons. As a result of many-body effects, the heptazine-based chains emit P-type delayed fluorescence at low temperature, originating from the robust triplet−triplet annihilation process.[24,25] Because of the spin-forbidden feature of triplet excitons, P-type delayed fluorescence usually possesses a much longer lifetime than prompt fluorescence, which thus could be distinguished from the fluorescence spectra at a long delay time (1 ms in this study). As displayed in Figure 3b, SC-HM exhibits weakened P-type delayed fluorescence with respect to pristine-HM, suggesting a lower triplet exciton concentration. Besides, the delayed fluorescence lifetimes are estimated to be ∼2.43 and 1.93 ms for pristine-HM and SC-HM, respectively, from the monomolecular exponential stage of the time-resolved delayed fluorescence spectra. The low triplet exciton concentration might originate from the low singlet exciton yield, whereas the reduced delayed fluorescence lifetime demonstrates the notably enhanced triplet exciton dissociation in SC-HM. Furthermore, the low exciton concentrations (for both singlet and triplet) would give rise to reduced excitonic interactions and thereby enhanced excited-species quantum yields.[24]

In view of the accelerated exciton dissociation, the charge carrier behavior in SC-HM is thereby distinct from that in pristine-HM. Figure 3c displays the Mott−Schottky curves,

DOI: 10.1021/jacs.6b12878
J. Am. Chem. Soc. 2017, 139, 2468−2473

where the positive slopes demonstrate the n-type features of both samples. On the other hand, the dramatically enhanced electron concentration in SC-HM can be concluded from its lower slope. On the basis of Mott−Schottky equation, we estimated the electron concentration of SC-HM to be ∼7.1-fold higher than that of pristine-HM. Moreover, the flat potential of SC-HM was determined to be −1.26 V vs Ag/AgCl (pH 6.6), which is more negative compared with pristine-HM (−1.02 V vs Ag/AgCl), suggesting the promoted reduction capacity of photogenerated electrons. The photocurrent−voltage curves (Figure 3d) suggest enhanced photocurrent response under negative bias, confirming enhanced photogeneration of hot electrons in SC-HM. In comparison, the approximate photocurrent responses under positive bias indicate similar hole behaviors in the two samples, in accordance with the supposed hole blocking in disordered chains. SC-HM exhibited significant promotion of the photocurrent transient response under a negative bias voltage (−0.4 V vs Ag/AgCl, pH 6.6) compared with pristine-HM, arising from its enhanced hot-electron generation. In addition, further experiments demonstrate the close relation of order−disorder interfaces and exciton dissociation, as the sample with higher content of order−disorder interfaces possesses a higher electron concentration (Figure S7). On the basis of the above results, we verified that the semicrystalline sample with alternating ordered and disordered chains could favor exciton dissociation, thereby promoting the electron concentration in the polymer matrix.

By virtue of the intriguing charge-carrier behavior, SC-HM is expected to be an efficient catalyst for electron-involved photocatalytic processes. Here the molecular oxygen activation property of SC-HM was first investigated by using 3,3′,5,5′-tetramethylbenzidine (TMB) as a probe molecule, whose oxidation can be evaluated by monitoring the absorbance peak around 380 nm. As illustrated in Figures 4a and S9, the continuous increase in absorbance clearly indicates the oxidation of TMB molecules by SC-HM, while pristine-HM possesses much lower oxygen activation ability. Moreover, the oxidation process exhibits highly oxygen-dependent character

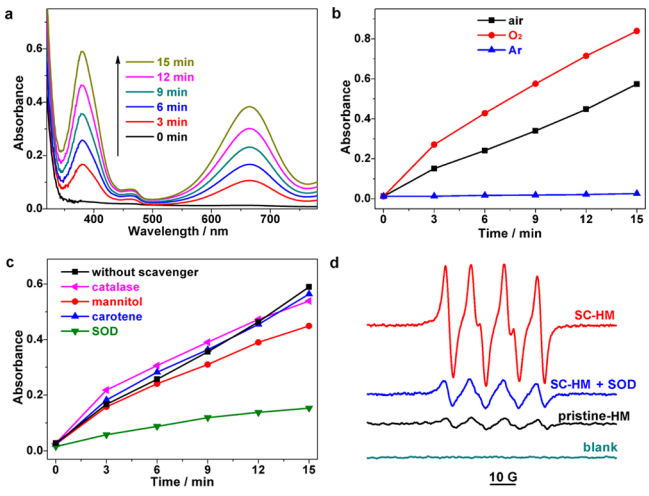

Figure 4. (a) Evolution of the absorption spectra of TMB oxidation in the presence of SC-HM in air. (b) Absorbance evolution of TMB oxidation with SC-HM monitored at 380 nm under different gas conditions. (c) Absorbance of TMB oxidation with SC-HM monitored at 380 nm in the presence of different scavengers. (d) ESR spectra of different samples in the presence of DMPO in methanol.

(Figure 4b), suggesting that the active species for TMB oxidation is derived from molecular oxygen activation process. To identify the generated reactive oxygen species, superoxide dismutase (SOD), mannitol, catalase, and carotene were employed as scavengers for superoxide radical ($O_2^{\bullet-}$), hydroxyl radical ($^{\bullet}OH$), hydrogen peroxide (H_2O_2), and singlet oxygen ($^1O_2$), respectively. Figure 4c illustrates that TMB oxidation is dramatically suppressed by SOD, while negligible effects are observed with the other scavengers. Therefore, $O_2^{\bullet-}$ is deduced to be the dominant species for TMB oxidation, which is in accordance with the band structure (Figure S10). In consideration of the involved photocatalytic mechanism, the significantly enhanced $O_2^{\bullet-}$ generation in SC-HM is ascribed to the notably promoted molecular oxygen reduction process arising from the effective hot-electron generation.

Electron spin resonance (ESR) analyses were further employed to verify the generated active species. 5,5-Dimethyl-1-pyrroline-*N*-oxide (DMPO) was selected as the trapping agent for the detection of $O_2^{\bullet-}$. As illustrated in Figure 4d, the sextet ESR signal that arises in the presence of SC-HM is in accordance with that of DMPO−OOH, a spin adduct derived from DMPO−$O_2^{\bullet-}$. The significant difference in intensity for the SC-HM and pristine-HM cases clearly demonstrates the enhanced $O_2^{\bullet-}$ generation with SC-HM. To gain a deeper understanding of the involved exciton dissociation, we eliminated the order−disorder interfaces of SC-HM by a rapid annealing treatment. As shown in Figure S11, the annealed sample possesses enhanced steady-state prompt fluorescence emission and reduced $O_2^{\bullet-}$ generation with respect to SC-HM, verifying the crucial role of order−disorder interfaces in exciton dissociation and thus hot-electron generation. Besides, SC-HM exhibits significant decreased $^1O_2$ generation with respect to pristine-HM (Figure S12), which further confirms the enhanced triplet exciton dissociation, in accordance with the delayed fluorescence measurements described above.

Benefiting from its intriguing molecular oxygen activation behavior, SC-HM is expected to be a potential photocatalyst for selective aerobic syntheses.[26] Herein, the selective alcohol oxidation reaction, which has been widely studied for the crucial role in the synthesis of fine chemicals and intermediates,[27] was employed to evaluate the photocatalytic performance of the obtained SC-HM sample. Table 1 lists the conversion rates and selectivities for the oxidation of a series of alcohols under the optimized conditions. As shown in entry 1, both SC-HM and pristine-HM could oxidize benzyl alcohol to benzaldehyde, but the former exhibits an ∼4.3-fold enhancement in conversion rate compared with the latter. Under an inert atmosphere (entry 2), the yield showed a significant reduction, suggesting that the oxidation is an oxygen-activation-mediated process. Moreover, the effect of substitutions on the aromatic ring was further studied. In terms of electron-withdrawing substituents (entries 3−6), the cases of halogen (F, Cl, Br) and nitro substituents were studied, in which SC-HM exhibited promoted yields with respect to pristine-HM. SC-HM also showed excellent performance in oxidation of benzylic alcohols with electron-donating substituents (methyl group; entry 7). The substitution position on the aromatic ring shows little influence on the oxidation process (entries 8 and 9). Besides, SC-HM also exhibits promoted performance in the case of a heterocyclic alcohol (entry 10). In general, the semicrystalline sample exhibits 3−6-fold improvements in aldehyde generation compared with the pristine counterpart.

DOI: 10.1021/jacs.6b12878
J. Am. Chem. Soc. 2017, 139, 2468−2473

Table 1. Selective Oxidation of Alcohols[a]

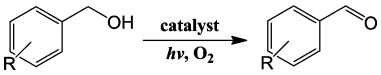

			pristine-HM		SC-HM	
entry	R	time/h	yield[b]	select.[c]	yield[b]	select.[c]
1	H	4	11	93	47	97
2[d]	H	4	5.5	99	7.3	99
3	*p*-F	3	13	98	62	96
4	*p*-Cl	3	19	95	51	96
5	*p*-Br	3	27	96	78	98
6	*p*-NO_2	3	6.7	95	38	97
7	*p*-Me	4	14	98	48	97
8	*m*-Cl	3	17	94	42	95
9	*o*-Me	3	10	96	46	98
10	2-pyridylmethanol	2	8.9	95	57	99

[a]Reaction conditions: alcohol (0.5 mmol), catalyst (10 mg), trifluorotoluene (2 mL), O_2 (1 atm), xenon lamp (50 W) without filter, 20 °C. [b]Determined by NMR analysis using 1,4-dicyanobenzene as the internal standard, mol %. [c]selectivity = $yield_{aldehyde}/conversion_{alcohol}$, mol %. [d]$N_2$, 1 atm.

It should be noted that although numerous catalysts have been established for photocatalytic alcohol oxidation, the yields of aldehydes are relatively low in pure photocatalytic processes (i.e., without the assistance of high temperature, high pressure, or cocatalysts). Here we have demonstrated SC-HM to be a promising catalyst for the selective alcohol oxidation reaction at atmospheric pressure and ambient temperature that exhibits performance comparable to that of the well-established photocatalysts.[28−30]

Moreover, wavelength-dependent measurements (Figure S13) demonstrate that although it exhibits weaker light absorption, SC-HM possesses much higher photocatalytic alcohol oxidation activity than pristine-HM, confirming that order−disorder-interface-induced exciton dissociation is the crucial factor for photocatalytic performance. Cycling measurements and structural characterizations (Figure S14) demonstrate that the conversion shows no obvious decrease within five-cycle tests and that the order−disorder structure is retained, indicating the excellent photocatalytic stability of SC-HM. Besides, selective oxidation of amines to imines, an extensively studied reaction by virtue of its chemical and biological significance,[31] was performed to further evaluate the catalytic performance of SC-HM (Table S2), and the semicrystalline sample exhibited much higher conversion and selectivity than the pristine counterpart. The metal-free SC-HM exhibits outstanding performance in selective oxidation, promising great prospects in industrial applications.

CONCLUSION

The excitonic aspects of photocatalytic processes in polymeric photocatalysts have been systematically investigated for the first time, offering an alternative strategy for hot-carrier harvesting. We propose that efficient hot-electron generation can be realized in novel semicrystalline heptazine-based melon as a result of accelerated exciton dissociation at order−disorder interfaces. The homojunction-like structure in the sample leads to consequent electron injection toward the ordered chains and hole blocking in the disordered chains, which hinders charge recombination, thereby facilitating electron migration toward the surface for photocatalytic processes. Profiting from hot-electron harvesting, the semicrystalline sample exhibits significantly promoted superoxide radical generation and improved selective alcohol oxidation. This work establishes a comprehensive understanding of photocatalytic processes from an excitonic perspective and puts forward a strategy for designing advanced polymeric photocatalysts via excitonic engineering.

ASSOCIATED CONTENT

Supporting Information

The Supporting Information is available free of charge on the ACS Publications website at DOI: 10.1021/jacs.6b12878.

Additional structural characterizations, electrochemical data, fitted fluorescence decay components, and photocatalytic measurements (PDF)

AUTHOR INFORMATION

Corresponding Authors

*zhxid@ustc.edu.cn

*yxie@ustc.edu.cn

ORCID

Xiaodong Zhang: 0000-0002-8288-035X

Yi Xie: 0000-0002-1416-5557

Notes

The authors declare no competing financial interest.

ACKNOWLEDGMENTS

This work was supported by the National Basic Research Program of China (2015CB932302), the National Natural Science Foundation of China (U1532265, U1632149, 21401181, 21331005, 11321503, and 91422303), the Youth Innovation Promotion Association of CAS (2017493), and the Fundamental Research Funds for the Central Universities (WK2060190027, WK2340000063, and WK6030000020). The authors thank Prof. Wensheng Yan (National Synchrotron Radiation Laboratory, USTC) for his helpful suggestions on XAS analyses.

REFERENCES

(1) Congreve, D.; Lee, J.; Thompson, N.; Hontz, E.; Yost, S.; Reusswig, P.; Bahlke, M.; Reineke, S.; Van Voorhis, T.; Baldo, M. *Science* **2013**, *340*, 334.

(2) Di, C.; Zhang, F.; Zhu, D. *Adv. Mater.* **2013**, *25*, 313.

(3) Deaton, J.; Switalski, S.; Kondakov, D.; Young, R.; Pawlik, T.; Giesen, D.; Harkins, S.; Miller, A.; Mickenberg, S.; Peters, J. *J. Am. Chem. Soc.* **2010**, *132*, 9499.

(4) He, Y.; Clark, G.; Schaibley, J.; He, Y.; Chen, M.; Wei, Y.; Ding, X.; Zhang, Q.; Yao, W.; Xu, X.; Lu, C.; Pan, J. *Nat. Nanotechnol.* **2015**, *10*, 497.

(5) Huang, M. H.; Mao, S.; Feick, H.; Yan, H. Q.; Wu, Y. Y.; Kind, H.; Weber, E.; Russo, R.; Yang, P. D. *Science* **2001**, *292*, 1897.

(6) Chen, X. B.; Shen, S. H.; Guo, L. J.; Mao, S. S. *Chem. Rev.* **2010**, *110*, 6503.

(7) Serpone, N.; Emeline, A. V. *J. Phys. Chem. Lett.* **2012**, *3*, 673.

(8) Chen, C.; Ma, W.; Zhao, J. *Chem. Soc. Rev.* **2010**, *39*, 4206.

(9) Ma, Y. Z.; Valkunas, L.; Dexheimer, S. L.; Bachilo, S. M.; Fleming, G. R. *Phys. Rev. Lett.* **2005**, *94*, 157402.

(10) Cao, Y.; Parker, I. D.; Yu, G.; Zhang, C.; Heeger, A. J. *Nature* **1999**, *397*, 414.

(11) Wang, X.; Maeda, K.; Thomas, A.; Takanabe, K.; Xin, G.; Carlsson, J. M.; Domen, K.; Antonietti, M. *Nat. Mater.* **2009**, *8*, 76.

(12) Thomas, A.; Fischer, A.; Goettmann, F.; Antonietti, M.; Muller, J.; Schlögl, R.; Carlsson, J. M. *J. Mater. Chem.* **2008**, *18*, 4893.

DOI: 10.1021/jacs.6b12878
J. Am. Chem. Soc. 2017, 139, 2468−2473

(13) Ong, W.; Tan, L.; Ng, Y.; Yong, S.; Chai, S. *Chem. Rev.* **2016**, *116*, 7159.
(14) Zhu, J.; Xiao, P.; Li, H.; Carabineiro, S. *ACS Appl. Mater. Interfaces* **2014**, *6*, 16449.
(15) Wang, H.; Jiang, S.; Chen, S.; Li, D.; Zhang, X.; Shao, W.; Sun, X.; Xie, J.; Zhao, Z.; Zhang, Q.; Tian, Y.; Xie, Y. *Adv. Mater.* **2016**, *28*, 6940.
(16) Paquin, F.; Latini, G.; Sakowicz, M.; Karsenti, P.-L.; Wang, L.; Beljonne, D.; Stingelin, N.; Silva, C. *Phys. Rev. Lett.* **2011**, *106*, 197401.
(17) Paquin, F.; Rivnay, J.; Salleo, A.; Stingelin, N.; Silva-Acuña, C. *J. Mater. Chem. C* **2015**, *3*, 10715.
(18) Hung, W. Y.; Fang, G. C.; Lin, S. W.; Cheng, S. H.; Wong, K. T.; Kuo, T. Y.; Chou, P. T. *Sci. Rep.* **2014**, *4*, 5161.
(19) Li, X. H.; Chen, J. S.; Wang, X. C.; Sun, J. H.; Antonietti, M. *J. Am. Chem. Soc.* **2011**, *133*, 8074.
(20) Cai, Y. Y.; Li, X. H.; Zhang, Y. N.; Wei, X.; Wang, K. X.; Chen, J. S. *Angew. Chem., Int. Ed.* **2013**, *52*, 11822.
(21) Li, X. H.; Antonietti, M. *Chem. Soc. Rev.* **2013**, *42*, 6593.
(22) Groenewolt, M.; Antonietti, M. *Adv. Mater.* **2005**, *17*, 1789.
(23) Paredes, J.; Villar-Rodil, S.; Solís-Fernández, P.; Martínez-Alonso, A.; Tascón, J. *Langmuir* **2009**, *25*, 5957.
(24) Steiner, F.; Vogelsang, J.; Lupton, J. *Phys. Rev. Lett.* **2014**, *112*, 137402.
(25) Parker, C.; Joyce, T. *Chem. Commun.* **1966**, *185*, 234.
(26) Colmenares, J.; Luque, R. *Chem. Soc. Rev.* **2014**, *43*, 765.
(27) Li, A.; Wang, T.; Chang, X.; Cai, W.; Zhang, P.; Zhang, J.; Gong, J. *Chem. Sci.* **2016**, *7*, 890.
(28) Yurdakal, S.; Palmisano, G.; Loddo, V.; Augugliaro, V.; Palmisano, L. *J. Am. Chem. Soc.* **2008**, *130*, 1568.
(29) Su, F.; Mathew, S. C.; Möhlmann, L.; Antonietti, M.; Wang, X.; Blechert, S. *Angew. Chem., Int. Ed.* **2011**, *50*, 657.
(30) Liang, S. J.; Wen, L. R.; Lin, S.; Bi, J. H.; Feng, P. Y.; Fu, X. Z.; Wu, L. *Angew. Chem., Int. Ed.* **2014**, *53*, 2951.
(31) Zhang, N.; Li, X.; Ye, H.; Chen, S.; Ju, H.; Liu, D.; Lin, Y.; Ye, W.; Wang, C.; Xu, Q.; Zhu, J.; Song, L.; Jiang, J.; Xiong, Y. *J. Am. Chem. Soc.* **2016**, *138*, 8928.

DOI: 10.1021/jacs.6b12878
J. Am. Chem. Soc. 2017, 139, 2468−2473